

## Pressure-driven phase transition mechanisms revealed by quantum chemistry: L-serine polymorphs

Denis A. Rychkov, Jernej Stare, Elena V. Boldyreva

### ELECTRONIC SUPPLEMENTARY MATERIAL

#### *Techniques*

##### *Solid State Calculations*

Periodic DFT calculations were performed by the program package VASP<sup>1-4</sup> using the functional of Perdew, Bruke and Ernzerhof (PBE)<sup>5</sup>, a plane-wave basis set with the kinetic energy cutoff of 500 eV and the Projector Augmented Wave atomic pseudopotentials<sup>6,7</sup>. The integrals in the reciprocal space were calculated on a Monkhorst-Pack mesh of  $8 \times 8 \times 4$   $k$ -points<sup>8</sup>. The effects of external pressure were enforced by the stress tensor (PSTRESS keyword) corresponding to a selected pressure value in the range between 0.0001 GPa and 8.1 GPa.

The models for all calculations were built on the basis of the experimental X-ray crystal and neutron powder diffraction data collected at different pressures. The CIF2Cell<sup>9</sup> script was used to convert the CIF structure files into VASP input files<sup>10</sup>. Energies and enthalpies of all the three polymorphs were calculated at multiple pressure points starting from the experimental structure but letting both the atomic positions and the unit cell parameters relax during energy optimization under the corresponding pressure (ISIF=3). The data for different polymorphs were used at different pressures, in agreement with the experimental information on which polymorph dominates at a selected pressure (see Fig. 2 in Results and Discussion). While geometry optimizations proceeded by using the first order Methfessel-Paxton method of setting partial occupancies of the wavefunctions (ISM EAR=1), energies of the optimized structures were recomputed at an improved accuracy by using the tetrahedron method with Bloch correction (ISM EAR=-5). Together with this, the aforementioned high plane wave cutoff and the dense  $k$ -point mesh are consistent with the high precision setting (PREC=HIGH) recommended for variable-cell calculations.

Fig.S1 shows that the discrepancy between relaxed cell parameters and experimental data never exceeded 3%. In these calculations full optimization at a corresponding pressure was used (*e.g.* starting guess from experimental structure at 4.8 GPa using programmed external pressure of 4.8 GPa).

To simulate a structure response to increasing or decreasing pressure, as compared with the starting point of the calculations, the unit cell parameters and atom positions were fully relaxed at the specified pressure value. In other words, to simulate structure of hypothetical polymorph I out of the structure stability range (*e.g.*, at 7.8 GPa) we used the previously optimized structure of form I at 4.8 GPa (obtained from the experimental data at 4.8 GPa) as starting point for another optimization at programmed external pressure of 7.8 GPa. To calculate a hypothetical structure of polymorph II at ambient pressure or higher than 8 GPa (out of the structural stability range) the structure was initially optimized at 7.0 GPa (where the phase was observed experimentally). Optimization at higher or lower pressures (0.0001GPa, 8.0, 8.1 GPa, etc.) was provided starting from this model using new programmed pressure (0.0001GPa, 8.0, 8.1 GPa, etc.). Thereafter, to calculate hypothetical structures of form III at pressures below 8.0 GPa initial atom coordinates were obtained from the structure optimized at 8.0 GPa and extended to new pressures (*e.g.* ambient, 1.0 GPa, 4.8 GPa, 5.0 GPa, etc.) As a result, hypothetical structure of every polymorph could be obtained and compared between all three forms at every desired pressure in terms of atom coordinates, energy and enthalpy. In this respect this approach was significantly different from the one in ref<sup>11</sup>.

The enthalpy was estimated as  $H = U_{\text{cryst}} + P \cdot V$ , where  $U_{\text{cryst}}$  is the crystal energy calculated by the above presented periodic DFT methodology. To estimate the energies of the crystal structure ( $U_{\text{cryst}}$ ) at variable pressure points, overall energy of the unit cell was calculated as ( $U_{\text{cryst}} = U_{\text{inter}} + U_{\text{intra}}$ ) without term separation.

All results obtained in this work were provided and discussed for enthalpies only Entropy was not taken into account for all three phases, despite that the  $T \cdot S$  term can influence Gibbs energy. The crystal symmetry does not change during phase transition I-III and no crucial changes in Raman spectra were observed<sup>12</sup>. We therefore assume the differences in the  $T \cdot S$  terms between polymorphs to be small. This approach provides a possibility to calculate enthalpies only, saving computational time with minor inaccuracy for Gibbs energy.

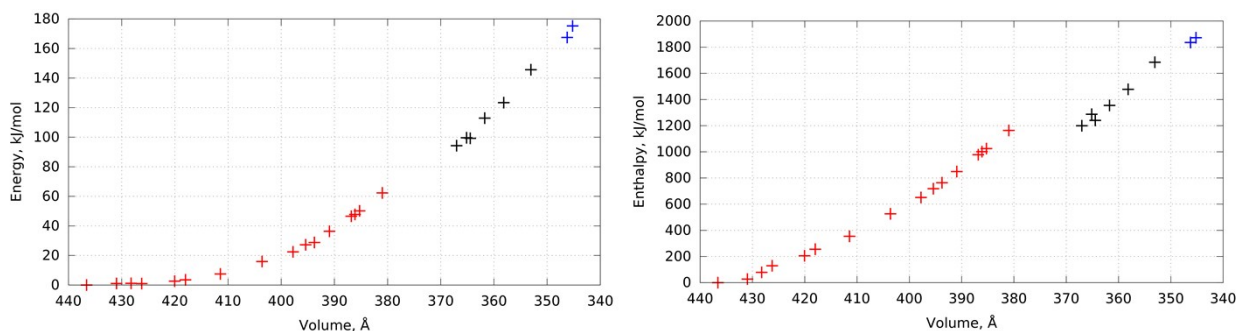


Fig. S1. Energy (a) and enthalpy (b) differences of L-serine structure vs. volume. Polymorphs experimentally observed at corresponding pressures are highlighted with color: L-serine I - red, L-serine II - black, L-serine III - blue. Internal crystal energies and enthalpies of all three polymorphs were calculated at multiple pressure points starting from the experimental data with relaxed atomic positions and cell parameters during optimization. Relative energies and enthalpies are plotted taking the minimal value in the set of calculations as zero.

### ***Accuracy Check of Solid State Calculations under Pressure***

The aforementioned concept was first tested for L-serine I in the pressure range 0 - 4.8 GPa, by comparing the structures obtained by “compressing the ambient-pressure structure by package tools” as implemented in VASP (PSTRESS option), with the structures based on real experimental data collected at non-ambient pressures. To estimate how sensitive this technique was to starting model, several crystal structures were used as a starting point to run the optimization: *i*) fully experimental (atom coordinates and cell parameters are taken from experiment), *ii*) only positions of hydrogen atoms optimized with unit cell parameters and coordinates of heavy atoms fixed, and *iii*) all atom coordinates and unit cell parameters fully optimized at starting pressure. During this straight optimization from 0.0001 GPa to 4.8 GPa different models at ambient pressure as starting ones were used. Results of all three optimization procedures with different starting structures were compared to each other and to the optimized structure at current pressure. The results of optimizing the structure at a higher pressure were insensitive to the choice of the starting structure at ambient pressure: the differences in all lattice parameters were within the 2.5% error limit\* (\* the only exception was parameter *c* for which discrepancy in case of optimization from 4.8 to ambient pressure was higher) (Fig. S1 in ESM). This is a high accuracy for pressure changes spanning four orders of magnitude.

The reverse optimization sequence (reducing pressure from 4.8 GPa to ambient using the 4.8 GPa models as the starting one) demonstrated slightly lower accuracy. However, in general, similar results were obtained (Fig. S1 in ESM, right column). Remarkably, as the pressure is decreased in the simulations, the unit cell does not expand as fast as it shrinks when pressure was increased.

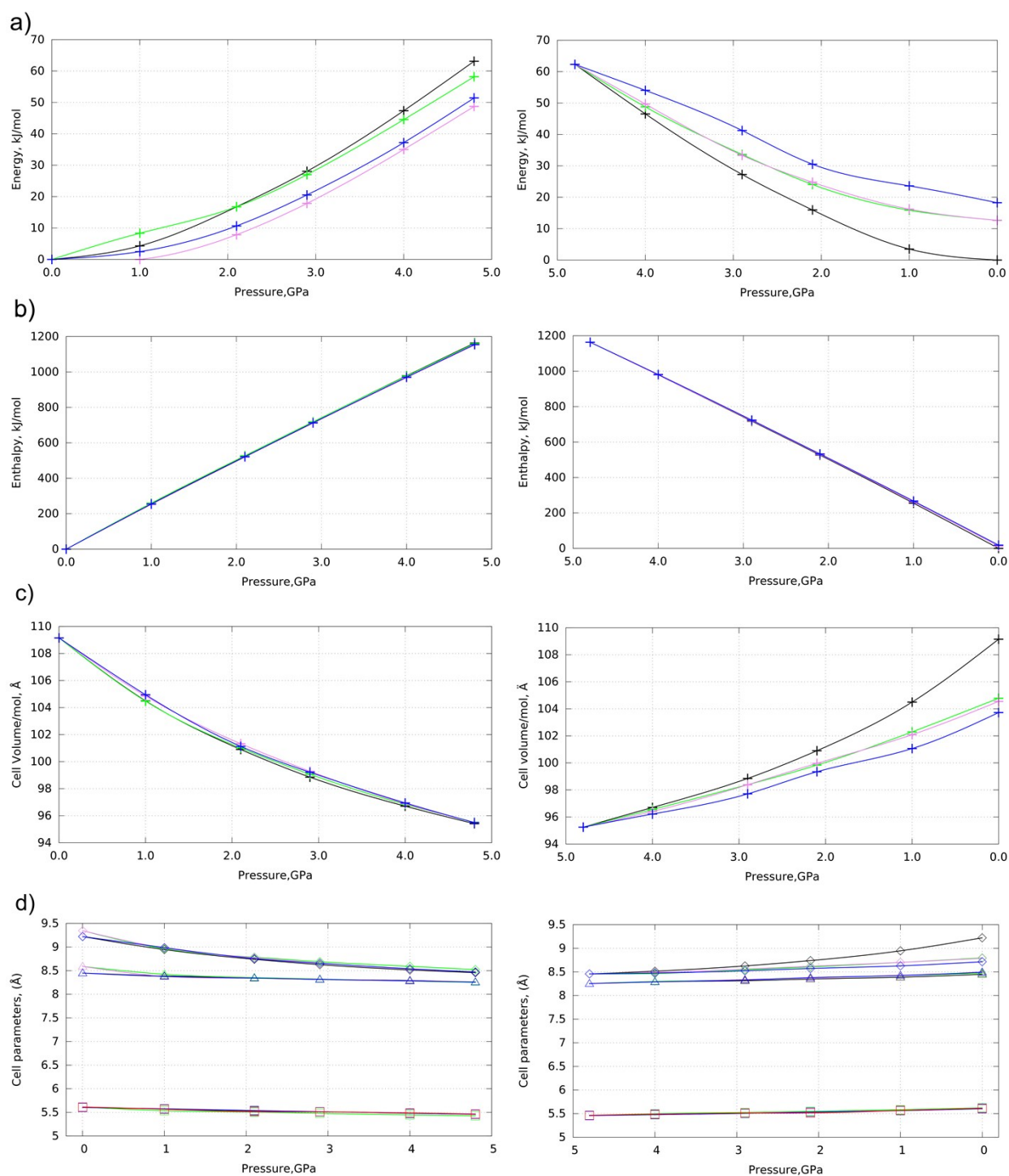


Fig.S2. Changes in different parameters characterizing L-serine I structure optimized at different pressure points (as computed by VASP) starting with different models; left - during direct (ambient  $\rightarrow$  4.8 GPa) optimization, right - during reverse (4.8 GPa  $\rightarrow$  ambient) optimization. Different models are: optimized at corresponding pressure - black (reference); only positions of hydrogen atoms optimized with unit cell parameters and coordinates of heavy atoms fixed - green; fully experimental (atom coordinates and cell parameters are taken from experiment) - violet, all atom coordinates and unit cell parameters preoptimized at initial pressure with subsequent optimization at corresponding pressure - blue. Values plotted vs. pressure: a) internal energy of the crystal ( $U_{\text{cryst}}$ ) difference, b) enthalpy difference, c) volume, d) unit cell parameters.

In the paper we mentioned that this feature can be a mere consequence of the way how the optimization code works, or resulting from implementation of dispersion forces, but it can be also a correct simulation of real changes in the structure, reflecting to some extent the hysteresis which is

observed experimentally across the I  $\rightarrow$  II phase transition experimentally. The I  $\rightarrow$  II transition is of a martensitic type, and, to start, it requires a significant value of “over-stressing”; a reverse transformation can occur at a lower pressure, which is closer to the equilibrium point than the point of direct transformation. Optimization of the structure after a change in pressure was more sensitive to the choice of the starting model, if the difference in pressure between the two points was smaller. Taking into account the good agreement between results obtained with different starting models, for all further studies we used optimized structures with relaxed unit cell and all atomic coordinates as a starting point, because in this case we could compare energies and enthalpies of predicted structures with those optimized at current pressure, and thus there were more opportunities for data extrapolation and corrections.

This methodology was applied in less detailed calculations for polymorph II (only for the pressure points at the higher and low limits of the stability range) and showed predicted structures to be close to the experimental ones. For phase III it was impossible to complete full validation because the structure of this polymorph was refined at two close pressure points only (8.0 and 8.1 GPa). This can affect the results, mostly in terms of volume expansion on reducing pressure. Moreover, no result correction (comparing predicted and experimental cell volumes) for polymorph III was possible because of the lack of experimental data.

Table S1. Calculated unit cell parameters for optimized structures of all three L-serine polymorphs in all experimental pressure range, including pressures beyond structural stability of corresponding forms. Optimization was provided using initial experimental data for L-serine I at 4.8 GPa, L-serine II at 5.7 GPa and L-serine III at 8.0 GPa.

Pressure, GPa	L-serine I				L-serine II				L-serine III			
	V, Å <sup>3</sup>	a, Å	b, Å	c, Å	V, Å <sup>3</sup>	a, Å	b, Å	c, Å	V, Å <sup>3</sup>	a, Å	b, Å	c, Å
ambient	415.40	5.606	8.500	8.718	399.28	5.746	7.071	9.827	393.23	5.786	6.948	9.781
0.1	414.25	5.601	8.490	8.711	398.64	5.744	7.066	9.821	391.93	5.783	6.932	9.776
0.3	411.92	5.593	8.476	8.689	396.74	5.739	7.048	9.809	390.40	5.778	6.920	9.764
0.5	407.04	5.576	8.440	8.648	394.97	5.733	7.031	9.799	388.32	5.771	6.898	9.755
0.8	405.79	5.571	8.433	8.638	392.34	5.722	7.009	9.782	386.64	5.764	6.886	9.741
1.0	406.34	5.570	8.437	8.647	390.43	5.718	6.985	9.775	384.22	5.759	6.857	9.729
1.4	402.30	5.554	8.410	8.613	388.17	5.712	6.966	9.756	381.73	5.750	6.833	9.716
2.1	397.60	5.533	8.380	8.575	382.00	5.689	6.903	9.727	376.91	5.732	6.786	9.690
2.6	393.38	5.516	8.351	8.540	379.33	5.676	6.887	9.704	372.58	5.722	6.738	9.664
2.9	390.32	5.503	8.323	8.522	377.10	5.669	6.860	9.696	371.32	5.717	6.726	9.656
3.1	390.01	5.502	8.324	8.516	375.69	5.663	6.848	9.687	370.08	5.712	6.715	9.648
3.5	388.58	5.495	8.317	8.502	373.74	5.655	6.828	9.679	368.00	5.705	6.694	9.635
4.0	384.50	5.476	8.284	8.476	370.55	5.645	6.798	9.656	364.71	5.692	6.664	9.614
4.1	384.55	5.477	8.287	8.473	369.88	5.641	6.792	9.653	363.98	5.692	6.656	9.608
4.2	382.69	5.467	8.268	8.466	369.51	5.639	6.789	9.652	363.57	5.691	6.651	9.605
4.8	380.99	5.458	8.253	8.457	366.11	5.630	6.756	9.625	360.59	5.680	6.625	9.582
5.0	380.35	5.456	8.251	8.449	364.74	5.623	6.744	9.617	359.28	5.673	6.615	9.574
5.2	378.33	5.449	8.242	8.424	363.87	5.623	6.734	9.609	358.37	5.673	6.602	9.568

5.4	377.48	5.446	8.236	8.417	362.91	5.620	6.725	9.602	357.28	5.669	6.592	9.561
5.7	375.74	5.440	8.224	8.399	361.31	5.609	6.715	9.593	355.62	5.662	6.576	9.551
6.3	372.08	5.424	8.200	8.366	358.45	5.601	6.685	9.574	352.45	5.648	6.547	9.531
7.2	367.52	5.402	8.170	8.327	353.38	5.584	6.634	9.539	346.26	5.615	6.500	9.487
8.0	363.46	5.388	8.150	8.277	349.47	5.575	6.589	9.513	346.26	5.615	6.500	9.487
8.2	362.66	5.385	8.147	8.266	349.15	5.567	6.593	9.512	346.26	5.615	6.500	9.487

### Energy-volume curves and bulk modulus calculations

Total energies of L-serine polymorphs were calculated versus the changes of cell volume as shown in Fig.S3. All three L-serine polymorphs structures optimized at ambient pressures were used as a starting point for energy calculations. These optimized unit cells were reduced by 5% at each direction (a, b, c) with the step of 1% and optimized with fixed volumes, but not the shape of the unit cell. Same procedure was performed for enlarged unit cells by 15% with the step of 1%. Energy-volume profiles were fitted with the 3<sup>rd</sup> order Birch-Murnaghan equation of state<sup>13,14</sup> -  $E = E_0 + 9/16 * V_0 * B_0 * (((V_0/V)^{(2/3)} - 1)^3 * B_0' + ((V_0/V)^{(2/3)} - 1)^2 * (6 - 4 * (V_0/V)^{(2/3)}))$

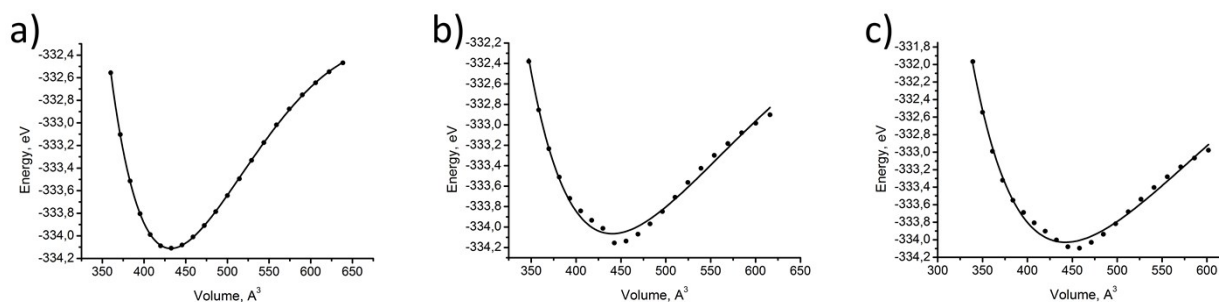


Fig.S3. The calculated internal crystal energy versus cell volume and the fitted parameters to the Birch–Murnaghan equation of state for a) L-serine I, b) – L-serine II, c) – L-serine III.

Different parameters of the fitting function are summarized at Table S2. L-serine I has higher values of Bulk modulus, as well as minimal volume ( $V_0$ ) and energy ( $E_0$ ). These parameters are in good agreement with conclusions obtained from individual H-bond simulation. This proves L-serine I being most stiff polymorph among L-serine structures, and confirm similarity of internal structures of polymorphs II and III (similar  $B_0$ ,  $E_0$ ,  $V_0$ ).

Table S2. The calculated bulk modulus, and the fitted parameters of the Birch–Murnaghan equation of state for L-serine polymorphs.

L-serine polymorph	$E_0$ , eV/cell	$B_0$ , eV/Å <sup>3</sup>	$B_0'$ , Å <sup>3</sup>	$V_0$ , Å <sup>3</sup>	Bulk modulus, GPa	Adjusted R-squared ( $R^2$ )
I	-334.111	0.146	8.869	432.148	23.4	0.99992
II	-334.065	0.092	7.271	440.248	14.7	0.98662
III	-334.028	0.087	6.672	442.313	13.9	0.99017

### Gas Phase Calculations

The Gaussian 09 program<sup>15</sup> was used to study intermolecular interactions between pairs of molecules. The calculations were performed using the M062X/6-311++G(2d,2p)<sup>16</sup> level of theory. All molecular pairs were extracted from crystal structures optimized at the corresponding pressure (see pressures in Table 2) and distance between these molecules was changed while their geometry and torsional alignment remained fixed. Calculations were performed using scan option with a step of 0.02 Å along H-bond (donor – acceptor vector) with molecular geometries fixed. These energies were plotted versus donor-acceptor distance.

It should be noted that the intermolecular potentials were calculated by the single point approach,

that is without geometry optimization. We are aware that structural relaxation is commonly performed in similar computational studies, and that the absence of relaxation represents a source of error<sup>17</sup>. However, for the present study it is essential that the alignment of molecules is preserved throughout the scan so that it mimics at the largest possible extent the alignment in the crystal. As geometry optimization would likely completely alter the alignment and structural features of the dimer due to the absence of crystalline environment holding the dimer in its place via multiple H-bonds, we are convinced that the single point strategy is the method of choice for the presently investigated problem.

All H-bonds were summarized (Table S1) and corresponding pairs of molecules were studied as described.

Table S3. Experimental data for the distances between non-hydrogen atoms, D ... A (Å) in possible intermolecular H-bonds in L-serine at ambient pressure, 4.2 GPa, 5.4 GPa, 7.5 GPa, 8.0 GPa.<sup>18</sup>

Hydrogen bond	Distance D...A (Å)				
	Amb. pres.	4.2	5.4	7.5	8.0
(1) N1-H3...O2 <sup>i</sup>	2.870(2)	2.81(1)	2.85(1)	2.84(1)	2.78(1)
(2) N1-H3...O1 <sup>i</sup>	3.112(2)	2.99(1)	3.21(1)	3.10(1)	3.12(1)
(3) N1-H4...O2 <sup>ii</sup>	2.874(2)	2.65(2)	2.90(2)	2.80(2)	2.97(2)
(4) N1-H4...O1 <sup>ii</sup>	2.841(2)	2.73(1)	2.67(1)	2.63(1)	2.64(1)
(5) O3-H7...O3 <sup>iv</sup>	2.9181(8)	2.767(4)			
(6) O3-H7...O2 <sup>v</sup>			2.66(1)	2.62(2)	2.65(1)
(7) O3-H7...O1 <sup>vi</sup>					2.90(2)
(8) N1-H3...O3 <sup>vii</sup>			3.42(2)	3.22(3)	3.04(2)

Symmetry codes: (i) -1+x, y, z (for 0 and 4.2 GPa) or 1+x, y, z (for 5.4, 7.5, 8.0 GPa); (ii) 1-x, 0.5+y, 1-z (for 0 and 4.2 GPa) or -x, 0.5+y, 0.5-z (for 5.4, 7.5, 8.0 GPa); (iii) -0.5+x, 0.5-y, 2-z (for 0 and 4.2 GPa) or 0.5 + x, 0.5-y, -z (for 5.4, 7.5, 8.0 GPa); (iv) -0.5 + x, 0.5-y, 1-z; (v) 0.5 + x, 0.5 -y, 1 - z; (vi) 0.5 - x, 1 - y, 0.5 + z; (vii) 1 - x, -0.5 + y, 0.5 - z.

The values marked grey exceed the limits commonly accepted for a H-bond, but they are given, to show differences and similarities of the structures at different pressures.

For all three polymorphs additional energy (in comparison to  $E_{\min}$  for donor-acceptor distance different from optimum) for every H-bond was calculated at pressures of 4.8, 5.4 and 8.0 GPa. The H-bond vector connecting the donor and acceptor atom can be mapped to x, y and z directions coinciding with unit cell vectors a, b and c, respectively. The energy contribution along each direction was calculated proportionally to the values of vector components. The highest overstrain for all three phases was found along the x vector (see Table S2).

Table S4. Hydrogen bonds under different pressure and their overstrain with respect to the optimal distance and energy

Polymorph #	Pressure, GPa	H-bond #	H-bond type	Min D...A Distance	Real D...A Distance	Ex	Ey	Ez	E, kJ/mol (overstrain)	Decrease after pressing
I	4.8	1_2*	N1-N3...O1,2 <sup>i</sup>	3.3	3.21	0,06	0,01	1,04	1,11	No
I	4.8	3	N1-H4...O2 <sup>ii</sup>	2.56	2.69	3,89	0,14	0,01	4,04	Yes
I	4.8	4	N1-H4...O1 <sup>ii</sup>	2.74	2.72`	0,01	0,18	0,01	0,20	No
<b>I</b>	<b>4.8</b>	<b>5</b>	<b>O3-H7...O3<sup>iv</sup></b>	<b>3.2</b>	<b>2.78</b>	<b>0,33</b>	<b>0,04</b>	<b>10,47</b>	<b>10,84</b>	<b>No</b>
II	5.4	1_2*	N1-N3...O1,2 <sup>i</sup>	3.38	3.34	0,01	0,01	0,15	0,17	No
II	5.4	3	N1-H4...O2 <sup>ii</sup>	2.70	2.85	4,05	0,05	0,56	4,66	Yes
II	5.4	4	N1-H4...O1 <sup>ii</sup>	2.74	2.64	0,04	1,34	0,01	1,39	No
II	5.4	6	O3-H7...O2 <sup>v</sup>	2.70	2.62	0,03	0,76	0,01	0,80	No
II	5.4	8	N1-H3...O3 <sup>vii</sup>	3.48	3.49	0,02	0,01	0,01	0,04	Yes

III	8.0	<b>1_2*</b>	<b>N1-N3...O1,2<sup>i</sup></b>	3.36	3.30	0,01	0,01	0,59	0,61	No
III	8.0	3	N1-H4...O2 <sup>ii</sup>	2.92	2.97	0,38	0,01	0,09	0,48	Yes
III	8.0	4	N1-H4...O1 <sup>ii</sup>	2.74	2.64	0,04	0,97	0,01	1,02	No
III	8.0	6	O3-H7...O2 <sup>v</sup>	2.75	2.65	0,06	1,01	0,01	1,08	No
III	8.0	7	O3-H7...O1 <sup>vi</sup>	2.90	2.64	1,93	1,56	1,05	4,54	No
III	8.0	8	N1-H3...O3 <sup>vii</sup>	3.22	3.04	1,35	0,20	0,61	2,16	No

H-bond with high overstrain are highlighted with bold.

Symmetry codes: (i)  $-1+x, y, z$  (for 0 and 4.2 GPa) or  $1+x, y, z$  (for 5.4, 7.5, 8.0 GPa); (ii)  $1-x, 0.5+y, 1-z$  (for 0 and 4.2 GPa) or  $-x, 0.5+y, 0.5-z$  (for 5.4, 7.5, 8.0 GPa); (iii)  $-0.5+x, 0.5-y, 2-z$  (for 0 and 4.2 GPa) or  $0.5+x, 0.5-y, -z$  (for 5.4, 7.5, 8.0 GPa); (iv)  $-0.5+x, 0.5-y, 1-z$ ; (v)  $0.5+x, 0.5-y, 1-z$ ; (vi)  $0.5-x, 1-y, 0.5+z$ ; (vii)  $1-x, -0.5+y, 0.5-z$ .

\* Bonds #3 and #4 are bifurcated and thus the distance between donor and centre between acceptors was used as a reference distance for all calculations for these bonds.

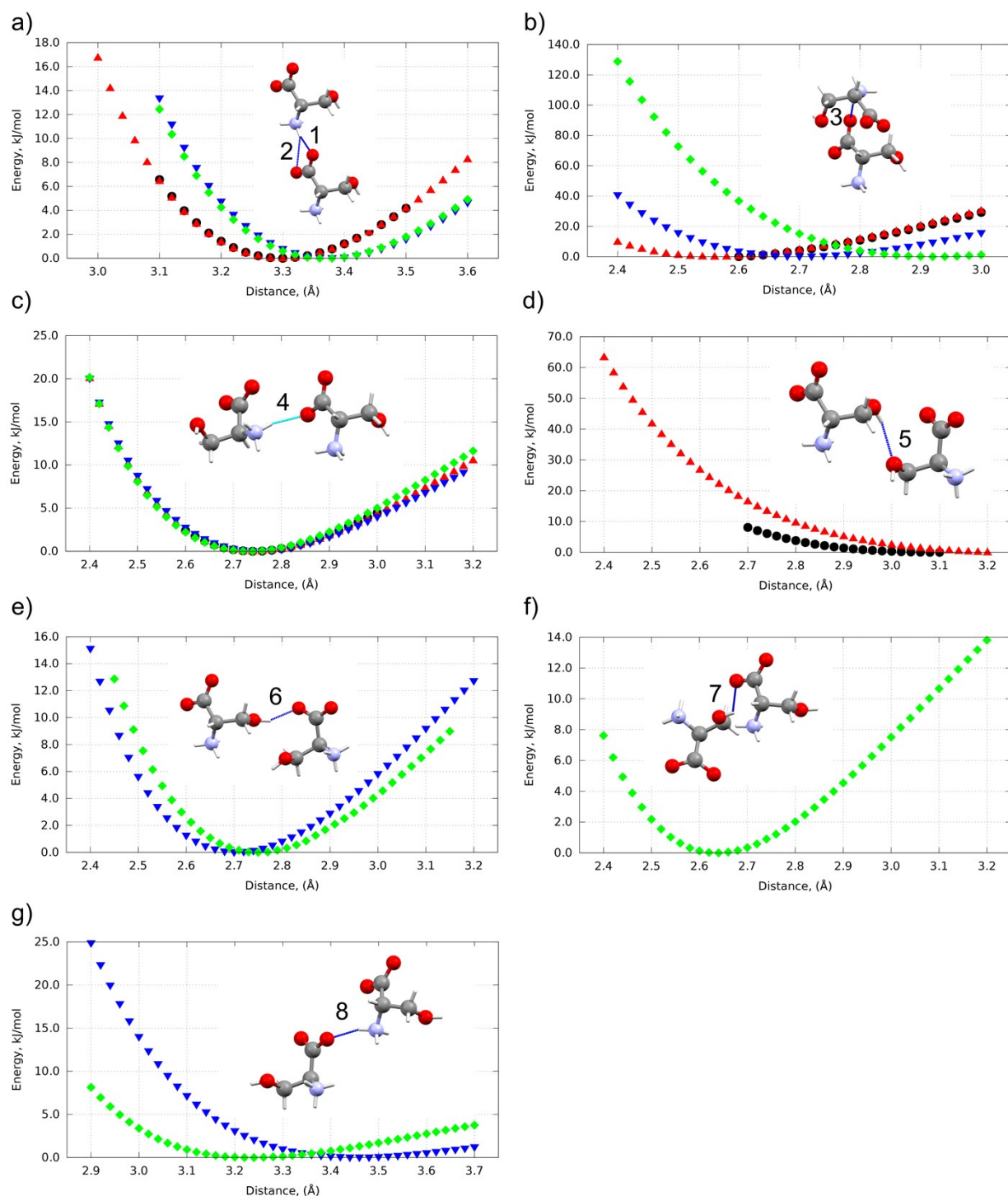


Fig.S4. Energy wells of pair-wise intermolecular interactions along H-bond. From left to right: a - H1,2 (H1 and H2 were estimated simultaneously - bifurcated H-bond), b - H3, c - H4, d - H5, e - H6, f - H7, g - H8. Ambient pressure - black, 4.8 GPa - red, 5.4 GPa - blue, 8.0 GPa - green. The profile changes for most H-bonds after the I→II phase transition. Numeration of H-bonds is as in Fig.3, main text, and Table S1 in ESM. Relative energies are plotted taking the minimal value in the set of calculations as zero.

#### ***Other programs used***

All crystal structures data were taken from Cambridge Structural Database (version 5.35, updated September 2014) using CONQUEST. Visualization and analysis of crystal structures was done using Mercury 3.5<sup>19</sup>, VMD 1.9.2<sup>20</sup>, and Jmol 13.0<sup>21</sup>. To create models for gas phase, Molden 5.4<sup>22</sup> software was used.

### Additional experimental data

Unit cell parameters plotted versus pressure. Data obtained from CCDC Database<sup>23</sup> based on experimental works<sup>11,18,24,25</sup>.

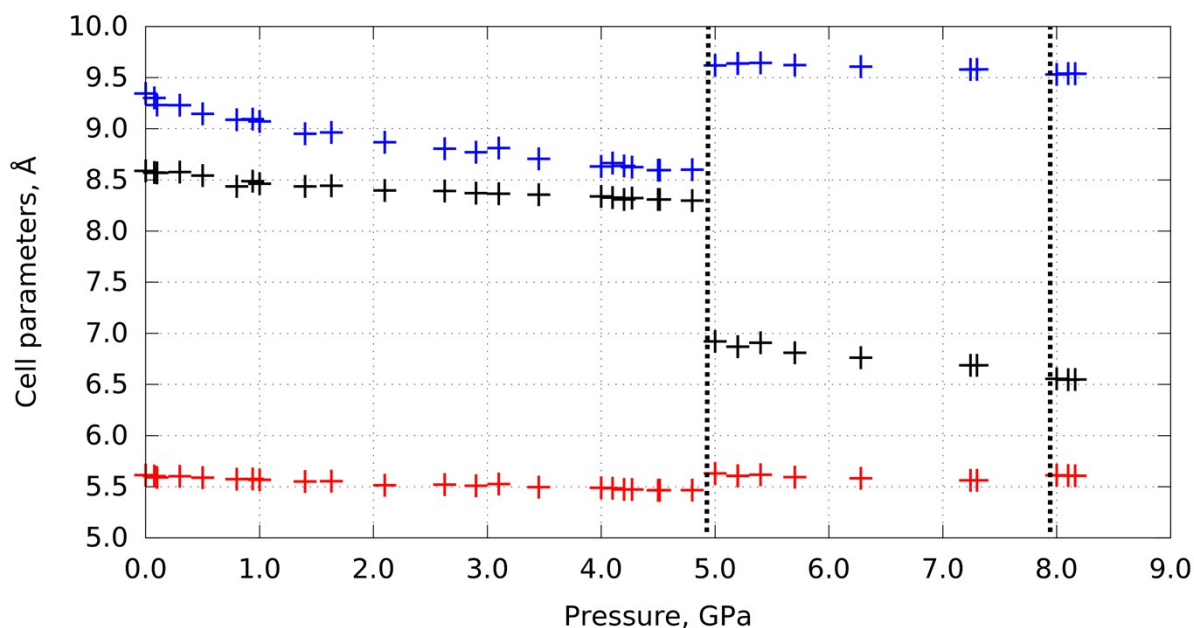


Fig.S5. Experimental unit cell parameters measured at various pressures<sup>18</sup>: *a* - red, *b* - black, *c* - blue.

### References

- 1 G. Kresse and J. Hafner, *Phys. Rev. B*, 1993, **47**, 558–561.
- 2 G. Kresse and J. Hafner, *Phys. Rev. B*, 1994, **49**, 14251–14269.
- 3 G. Kresse and J. Furthmüller, *Phys. Rev. B*, 1996, **54**, 11169–11186.
- 4 G. Kresse and J. Furthmüller, *Comput. Mater. Sci.*, 1996, **6**, 15–50.
- 5 J. P. Perdew, K. Burke and M. Ernzerhof, *Phys. Rev. Lett.*, 1996, **77**, 3865–3868.
- 6 P. E. Blöchl, *Phys. Rev. B*, 1994, **50**, 17953–17979.
- 7 G. Kresse and D. Joubert, *Phys. Rev. B*, 1999, **59**, 1758–1775.
- 8 H. J. Monkhorst and J. D. Pack, *Phys. Rev. B*, 1976, **13**, 5188–5192.
- 9 T. Björkman, *Comput. Phys. Commun.*, 2011, **182**, 1183–1186.
- 10 S. Grimme, *J. Comput. Chem.*, 2006, **27**, 1787–99.
- 11 P. A. Wood, D. Francis, W. G. Marshall, S. A. Moggach, S. Parsons, E. Pidcock and A. L. Rohl, *CrystEngComm*, 2008, **10**, 1154.

- 12 E. N. Kolesnik, S. V. Goryainov and E. V. Boldyreva, *Dokl. Phys. Chem.*, 2005, **404**, 169–172.
- 13 F. D. Murnaghan, *Am. J. Math.*, 1937, **59**, 235–260.
- 14 F. Birch, *Phys. Rev.*, 1947, **71**, 809–824.
- 15 Gaussian, M. J. Frisch, G. W. Trucks, H. B. Schlegel, G. E. Scuseria, M. A. Robb, J. R. Cheeseman, G. Scalmani, V. Barone, B. Mennucci, G. A. Petersson, H. Nakatsuji, M. Caricato, X. Li, H. P. Hratchian, A. F. Izmaylov, J. Bloino, G. Zheng, J. L. Sonnenberg, M. Hada, M. Ehara, K. Toyota, R. Fukuda, J. Hasegawa, M. Ishida, T. Nakajima, Y. Honda, O. Kitao, H. Nakai, T. Vreven, J. A. Montgomery, J. E. P. Jr., F. Ogliaro, M. Bearpark, J. J. Heyd, E. Brothers, K. N. Kudin, V. N. Staroverov, R. Kobayashi, J. Normand, K. Raghavachari, A. Rendell, J. C. Burant, S. S. Iyengar, J. Tomasi, M. Cossi, N. Rega, J. M. Millam, M. Klene, J. E. Knox, J. B. Cross, V. Bakken, C. Adamo, J. Jaramillo, R. Gomperts, R. E. Stratmann, O. Yazyev, A. J. Austin, R. Cammi, C. Pomelli, J. W. Ochterski, R. L. Martin, K. Morokuma, V. G. Zakrzewski, G. A. Voth, P. Salvador, J. J. Dannenberg, S. Dapprich, A. D. Daniels, Ö. Farkas, J. B. Foresman, J. V. Ortiz, J. Cioslowski, and D. J. Fox and W. C. G. Inc.", 2009.
- 16 Y. Zhao and D. G. Truhlar, *Theor. Chem. Acc.*, 2008, **120**, 215–241.
- 17 A. V Shishkina, V. V Zhurov, A. I. Stash, M. V Vener, A. A. Pinkerton and V. G. Tsirelson, *Cryst. Growth Des.*, 2013, **13**, 816–828.
- 18 E. V. Boldyreva, H. Sowa, Y. V. Seryotkin, T. N. Drebuschak, H. Ahsbahs, V. Chernyshev and V. Dmitriev, *Chem. Phys. Lett.*, 2006, **429**, 474–478.
- 19 C. F. Macrae, P. R. Edgington, P. McCabe, E. Pidcock, G. P. Shields, R. Taylor, M. Towler and J. van de Streek, *J. Appl. Crystallogr.*, 2006, **39**, 453–457.
- 20 W. Humphrey, A. Dalke and K. Schulten, *J. Mol. Graph.*, 1996, **14**, 33–38.
- 21 J. an open-source J. viewer for chemical structures in 3D. [Http://www.jmol.org/](http://www.jmol.org/), .
- 22 G. Schaftenaar and J. H. Noordik, *J. Comput. Aided. Mol. Des.*, 2000, **14**, 123–134.
- 23 C. R. Groom, I. J. Bruno, M. P. Lightfoot and S. C. Ward, *Acta Crystallogr. Sect. B Struct. Sci. Cryst. Eng. Mater.*, 2016, **72**, 171–179.
- 24 S. A. Moggach, W. G. Marshall and S. Parsons, *Acta Crystallogr. Sect. B Struct. Sci.*, 2006, **62**, 815–825.
- 25 T. N. Drebuschak, H. Sowa, Y. V. Seryotkin, E. V. Boldyreva and H. Ahsbahs, *Acta Crystallogr. Sect. E Struct. Reports Online*, 2006, **62**, o4052–o4054.